The Astrophysical Journal, 845:64 (11pp), 2017 August 10 https://doi.org/10.3847/1538-4357/aa7f28

Self-gravity in Magnetized Neutrino-dominated Accretion Disks

Narjes Shahamat[1] and Shahram Abbassi[1,2]
[1] Department of Physics, School of Science, Ferdowsi University of Mashhad, Mashhad, P.O. Box 91775-1436, Iran; abbassi@um.ac.ir
[2] School of Astronomy, Institute for Studies in Theoretical Physics and Mathematics, P.O. Box 19395-5531, Tehran, Iran
Received 2017 March 1; revised 2017 June 16; accepted 2017 July 8; published 2017 August 11

Abstract

In the present work we study self-gravity effects on the vertical structure of a magnetized neutrino-dominated accretion disk as a central engine for gamma-ray bursts (GRBs). Some of the disk physical timescales that are supposed to play a pivotal role in the late-time evolutions of the disk, such as viscous, cooling, and diffusion timescales, have been studied. We are interested in investigating the possibility of the occurrence of X-ray flares, observed in late-time GRBs' extended emission through the "magnetic barrier" and "fragmentation" processes in our model. The results lead us to interpret self-gravity as an amplifier for Blandford–Payne luminosity (BP power) and the generated magnetic field, but a suppressor for neutrino luminosity and magnetic barrier processes via highlighting the fragmentation mechanism in the outer disk, especially for the higher mass accretion rates.

Key words: accretion, accretion disks – magnetic fields – magnetohydrodynamics (MHD)

1. Introduction

Gamma-ray bursts (GRBs) are a sudden release of about 10^{51}–10^{54} erg of energy in a volume with a radius of less than 100 km, which last from 0.01 to 100 s (for reviews, see Piran 2004; Meszaros 2006; Nakar 2007; Gehrels et al. 2009; Kumar & Zhang 2015). According to the duration time T_{90}, which is defined as the time interval over which 90% of the total background-subtracted counts are observed, GRBs are usually separated into two classes: long GRBs (LGRBs; $T_{90} > 2$ s), whose existence emanates from the core collapse of massive stars (Kouveliotou et al. 1993; Woosley 1993; Paczynski 1998; Hjorth et al. 2003), and short GRBs (SGRBs; $T_{90} < 2$ s), whose origins are thought to be the coalescence of neutron stars (NSs) or NS–black hole binary systems (Eichler & Cheng 1989; Narayan et al. 1992; Kouveliotou et al. 1993; Fryer & Woosley 1998). All these scenarios result in a hyperaccreting, spinning, stellar-mass black hole with a mass accretion rate in the range of 0.01–$10 M_{\odot}/s$, surrounded by an accretion disk of several solar masses (Popham et al. 1999; Gu et al. 2006; Liu et al. 2007), which is hot and dense enough to be cooled via neutrino pair annihilation on the surface and called neutrino-dominated accretion flow (NDAF), or a magnetar (Usov 1992; Dai et al. 2006; Yu et al. 2013). In addition to the NDAF model, the Blandford–Znajek (BZ) mechanism (Blandford & Znajek 1977) is considered another promising candidate to effectively cool this hyperaccretion disk (Meszaros & Rees 1997).

In spite of these proposed mechanisms, there is still great ambiguity about the nature of GRB's central engine. Considering the neutrino opacity, the neutrino–antineutrino annihilation is not efficient enough to power the energetic short–hard GRBs (e.g., GRB 080913). The NDAF model is also unable to fuel the X-ray flares observed in GRBs' emission by *Swift* (Fan et al. 2005). On the other hand, Narayan, Paczynski, and Piran (Narayan et al. 1992) showed that the magnetic field can reach 10^{12} G immediately after the disk formation and increases up to 10^{15}–10^{16} G owing to the shearing action of the differentially rotating disk. Hence, the idea of an MHD process strengthened in later works (e.g., Di Matteo et al. 2002; Fan et al. 2005; Shibata et al. 2007). Furthermore, such a process might be a reliable alternative for X-ray flares through a magnetic barrier (see Proga & Zhang 2006). Accordingly, it seems rather inevitable to regard the effects of magnetic field in the NDAF model.

On the other hand, the high mass density of NDAFs ($\rho \sim 10^{10}$ g cm^{-3}) motivates us to study the influence of self-gravity in the dynamical structure of these systems. With the idea that flares have something to do with what is in common between SGRBs and LGRBs (i.e., hyperaccretion disk), Perna et al. (2006) argued that the gravitational instability leads to either large-amplitude changes in the inner accretion rate or complete fragmentation of the disk followed by a relatively slow inspiral of fragments toward the black hole. This results in a less powered jet, which can be the seed for the late-time flares. Thus, taking the effects of self-gravity into account seems to give us a more realistic insight into the NDAFs' structure and their evolution.

Some authors have studied the vertical structure of optically thick disks, including NDAFs (e.g., Gu et al. 2007, 2009; Jiao et al. 2009; Liu et al. 2010a). The impact of vertical self-gravity has also been considered by Liu et al. (2014). From the magnetic points of view, the study of NDAF structure has been developed through several works (e.g., Lei et al. 2009; Xie et al. 2009; Cao et al. 2014). However, combining these two significant physical features has not yet been considered. For a more comprehensive discussion of NDAF studies, we refer readers to a recent review by Lui et al. (2017). In this paper, motivated by the above ideas, we have focused on the influence of vertical self-gravity on magnetized NDAFs.

In Section 2.1, the basic equations and assumptions are included. In order to consider the effects of self-gravity and study "magnetic barrier" and "fragmentation" probabilities, we introduce the Toomre parameter and viscous, diffusion, and cooling timescales in Sections 2.2 and 2.3. In addition, neutrino and Blandford–Payne (BP) luminosities are included in Section 2.4. Section 3 represents our numerical outcomes, and Section 4 contains some estimates in order to provide a comparison to the observations. The final discussion, including the main conclusions, is given in Section 5.

2. Physical Model

2.1. Basic Formalism

We study a steady and axisymmetric magnetized NDAF ($\partial/\partial t = 0$, $\partial/\partial\phi = 0$) in which self-gravity has been taken into account, vertically. Considering the magnetic field influence on both large scales (magnetic braking mechanism) and small scales (viscous dissipation effects), through which the disk's rotational energy extraction and angular momentum transfer happen (Blandford 1976; Blandford & Payne 1982; Balbus & Hawley 1991; Lee et al. 2000), yields the following results for the continuity and angular momentum equations:

$$\dot{M} = -2\pi R\Sigma v_R = \text{constant}, \tag{1}$$

$$\dot{M} = \frac{2\pi\alpha R^2\Pi}{\Omega_k R^2 - j} + \frac{B_\phi B_z R^2}{\frac{\partial}{\partial R}(R^2\Omega_k)}, \tag{2}$$

where we have followed the approach of Lee et al. (2000) and Xie et al. (2009) in order to include magnetic braking effects. Note that $\dot{M}$ is the mass accretion rate, v_R is the radial velocity, $\Omega_k = (GM/R)^{1/2}/(R - R_g)$ is the Keplerian angular velocity, G is the gravitational constant, $R_g = 2GM/c^2$ is the Schwarzschild radius, $j = 1.8cR_g$ is an integration constant representing the angular momentum of the innermost stable circular orbit, α is the magnetic viscosity parameter (Shakura & Sunyaev 1973; Pringle 1981), and B_R, B_ϕ, and B_z are the three components of the magnetic field. Furthermore, Σ and Π are the surface density and vertically integrated pressure, respectively, defined as

$$\Sigma = 2\int_0^H \rho dz, \tag{3}$$

$$\Pi = 2\int_0^H p dz, \tag{4}$$

in which p and ρ are the disk pressure and mass density, respectively, and the speed of sound is further defined as $c_s = \left(\frac{\Pi}{\Sigma}\right)^{1/2} \approx \left(\frac{p_0}{\rho_0}\right)^{1/2}$, where the zero index is related to the equatorial plane quantities. The half thickness of the disk is denoted by $H = \frac{\Sigma}{2\rho_0}$ here.

The energy balance equation consists of viscous heating, neutrino and advective cooling, and the fraction of rotational energy extracted by magnetic braking effects (Xie et al. 2009),

$$Q_{\rm vis} = Q_{\rm adv} + Q_\nu^- + Q_B^-. \tag{5}$$

The viscous heating rate is

$$Q_{\rm vis} = \frac{1}{2\pi}\dot{M}\Omega_K^2 fg, \tag{6}$$

where $f = 1 - j/\Omega_K R^2$ and $g = -d\ln\Omega_K/d\ln R$. The advective cooling rate is

$$Q_{\rm adv} = \frac{1}{2\pi}\frac{\xi\dot{M}c_s^2}{R^2}, \tag{7}$$

in which $\xi = 3/2$ is a dimensionless quantity of the order of unity (e.g., Kato et al. 2008). The neutrino cooling rate is expressed by a bridging formula (e.g., Di Matteo et al. 2002; Kohri et al. 2005) as follows:

$$Q_\nu = \sum_i \frac{(7/8)\sigma T^4}{(3/4)\left[\frac{\tau_{\nu_i}}{2} + \frac{1}{\sqrt{3}} + \frac{1}{3\tau_{a,\nu_i}}\right]}, \tag{8}$$

where σ is the Stefan–Boltzmann constant, T is the temperature, and τ_{ν_i} is the total optical depth for neutrinos, including the absorption optical depth τ_{a,ν_i} and scattering optical depth τ_{s,ν_i},

$$\tau_{\nu_i} = \tau_{a,\nu_i} + \tau_{s,\nu_i}, \tag{9}$$

where $i = 1, 2, 3$ refers to the three kinds of leptons, ν_e, ν_μ, and ν_τ. The main absorption processes include the electron–positron pair annihilation and Urca processes (e.g., Narayan et al. 2001; Di Matteo et al. 2002; Liu et al. 2014), and the corresponding optical depths can be written as

$$\tau_{a,\nu_i} = 2.5 \times 10^{-7} T_{11}^5 H, \tag{10}$$

$$\tau_{a,\nu_e} = 2.5 \times 10^{-7} T_{11}^2 X_{\rm nuc}\rho_{10} H, \tag{11}$$

where $T_{11} = \frac{T}{10^{11}}K$, $\rho_{10} = \frac{\rho}{10^{10}}\,{\rm g\,cm^{-3}}$, and $X_{\rm nuc}$ is the mass fraction of free nucleons approximately given by (e.g., Liu et al. 2014)

$$X_{\rm nuc} = \min\{1, 295.5\rho_{10}^{-3/4}T_{11}^{9/8}\exp(-0.8209/T_{11})\}. \tag{12}$$

The scattering optical depth by nucleons can be given by

$$\tau_{s,\nu_i} = 2.7 \times 10^{-7} T_{11}^2\rho_{10} H. \tag{13}$$

Following Lee et al. (2000) and Xie et al. (2009), Q_B^- can be calculated as $\Omega d\tau/ds$, in which $d\tau$ is the torque exerted by the annular ring with width dR of the disk due to the Lorentz force ($ds = 2\pi\, RdR$). Thus, we have

$$Q_B^- = 2R\Omega(B_\phi B_z/4\pi). \tag{14}$$

The equation of state (EOS) is written as (e.g., Di Matteo et al. 2002; Liu et al. 2014)

$$p = p_{\rm gas} + p_{\rm rad} + p_{\rm deg} + p_\nu. \tag{15}$$

The gas pressure from the free nucleons and α-particles is $p_{\rm gas} = \frac{\rho k_B T}{m_p}\frac{1+3X_{\rm nuc}}{4}$, where a is the radiation constant, T is the disk temperature, and k_B is the Stephan–Boltzmann constant (see Woosley & Baron 1992; Qian & Woosley 1996). The radiation pressure is $p_{\rm rad} = \frac{1}{3}aT^4$. In degeneracy term $p_{\rm deg} = \frac{2\pi hc}{3}\left(\frac{3\rho}{16\pi m_u}\right)^{4/3}$, where m_u is the mean mass of a nucleon and h is the Planck constant, only the degeneracy of electrons (rather than both electrons and nucleons) has been considered. Generally speaking, the degeneracy pressure is important at high-density and low-temperature regimes. Such regimes inevitably appear in very massive disks, like NDAFs. The last term denotes the neutrino pressure $P_\nu = \frac{u_\nu}{3}$, in which $u_\nu = \sum_i \frac{(7/8)aT^4(\tau_{\nu_i}/2 + 1/\sqrt{3})}{\tau_{\nu_i}/2 + 1/\sqrt{3} + 1/(3\tau_{a,\nu_i})}$ is the neutrino energy density (Di Matteo et al. 2002; Kohri et al. 2005). Giving the correct behavior in the limit of both small and large τ_{ν_i} and τ_{a,ν_i}, this relation was derived in the context of radiative transport and assumes that opacities and emissivities are independent of the z coordinate. However, this assumption might be less accurate

for the neutrino transport, where all cross sections are a function of temperature and hence of the vertical disk structure.

Moreover, we consider the polytropic EOS in vertical direction $p = K\rho^{4/3}$, where K is a constant (Liu et al. 2014).

Another balance equation of which we are in need is the hydrostatic balance equation in the vertical direction, which reads

$$4\pi G\Sigma_z + \frac{\partial \Psi}{\partial z} + \frac{1}{\rho}\frac{\partial p}{\partial z} + \frac{1}{8\pi\rho}\left(\frac{\partial B_\phi^2}{\partial z} + \frac{\partial B_R^2}{\partial z}\right) - \frac{1}{4\pi\rho}B_R\frac{\partial B_z}{\partial R} = 0. \quad (16)$$

In the case of $\Sigma_z = \int_0^z \rho dz'$ (Paczynski 1978a, 1978b) being slowly varied with radius, the first term represents the vertical self-gravity. The two last terms are the ϕ-component of Lorentz force, as well. Now we adopt the pseudo-Newtonian potential, written by Paczynski and Wiita (Paczynsky & Wiita 1980), in order to mimic the effective potential of a Schwarzschild black hole:

$$\Psi = \frac{-GM}{\sqrt{R^2 + z^2} - R_g}. \quad (17)$$

The consideration of Gauss's law, $\nabla . B = 0$, the polytropic EOS, and Equation (17) leads to

$$4\pi G\Sigma_z + \Omega^2 z + \frac{4}{3\rho^{2/3}}k\frac{\partial \rho}{\partial z} - \frac{1}{4\pi\rho}\left[\left(\frac{\partial (B_R B_z)}{\partial R} + B_z\frac{\partial B_z}{\partial z}\right) + \frac{B_z B_R}{R} - \frac{1}{2}\frac{\partial}{\partial z}(B^2 - B_z^2 + B_R^2 + B_\phi^2)\right] = 0. \quad (18)$$

As the next step, we make use of the local shearing sheet simulations of accretion disks, in which it was found that the magnetic field components have somewhat standard ratios (Xie et al. 2009). For example, Table 2 of Stone et al. (1996) gives (note that their x, y, z correspond to R, ϕ, z)

$$B_R^2 \simeq \frac{1}{10}B_\phi^2, \quad (19)$$

$$B_z^2 \simeq \frac{1}{20}B_\phi^2, \quad (20)$$

and

$$B_z B_R \simeq 4\pi \times 10^{-5} p. \quad (21)$$

We also need to have some additional considerations, essential for the hydrostatic balance equation to be vertically integrated, as follows: mathematically speaking, the magnetic pressure, $p_{\rm mag} = B^2/8\pi$, can be written as

$$B^2/8\pi < p + B^2/8\pi,$$

which yields

$$p_{\rm mag} = \beta(p + B^2/8\pi) \text{ with } \beta < 1.$$

Therefore,

$$B_0^2 = 8\pi\frac{\beta_1}{1-\beta_1}p_0 \quad (22)$$

and

$$B_H^2 = 8\pi\frac{\beta_2}{1-\beta_2}p_H. \quad (23)$$

On the other hand,

$$B_{z0}^2 < B_0^2,$$

so

$$B_{z0}^2 = \gamma_1 B_0^2 \text{ with } \gamma_1 < 1 \quad (24)$$

and similarly

$$B_{zH}^2 = \gamma_2 B_H^2 \text{ with } \gamma_2 < 1. \quad (25)$$

As the last step, we use the Taylor expansion for density about "$z = 0$" up to a second-order term (as a good approximation for thin accretion disks), besides the reflection symmetry for density, and consider $\rho_H = \rho_0 \exp(-1/2)$ (Cao et al. 2014) ("H" index refers to the surface quantities). Thus, we have

$$\rho = \rho_0 + \alpha_1\frac{z^2}{2H^2},$$

where

$$\alpha_1 = 2\rho_0(e^{-1/2} - 1).$$

Regarding all the above considerations, in addition to $p_H = p_0 \exp(-1/2)$, one can integrate Equation (18) over "z," which yields

$$2\pi G\rho_0^2 H^2 + \Omega^2\frac{\rho_0 H^2}{2} + p_0(e^{-1/2} - 1) - 10^{-5}H\frac{dp_0}{dR} - 2p_0\left(\frac{\beta_2}{1-\beta_2}\gamma_2 e^{-2/3} + \frac{\beta_1}{1-\beta_1}\gamma_1\right) - \frac{10^{-5}p_0 H}{R} + p_0\left(\frac{\beta_2}{1-\beta_2}e^{-2/3} + \frac{\beta_1}{1-\beta_1}\right) = 0. \quad (26)$$

For the sake of simplicity, we ignore the zero indices.

Now we are left with eight unknowns (v_R, ρ, p, h, T, and three components of magnetic field) and seven equations (i.e., Equations (1), (2), (5), (15), (19), (20), and (26)). Thus, we are in need of one more equation and a boundary condition for the disk pressure, since Equation (26) is a differential one. The latter requirement can be removed by applying the numerical results obtained by, for example, Popham et al. (1999), who estimate a value of about 10^{30} erg cm^{-3} for the pressure in the inner regions of such hyperaccretion disks. Furthermore, the magnetic viscosity equation, as the last required equation, seems to be worthwhile here:

$$\frac{B_R B_\phi}{4\pi} = -\frac{3}{2}\alpha p. \quad (27)$$

In order to achieve a better understanding of the effects of magnetic field and self-gravity through an analogy among the three cases (self-gravitating magnetized NDAFs, magnetized case, and self-gravitating case), we may get the required equations by ignoring the terms associated with the magnetic field and self-gravity in the above-mentioned equations. For instance, considering the hydrostatic balance Equation (16), the magnetized NDAF can be obtained by ignoring the first term

(which reflects the self-gravity impact):

$$\frac{\partial \Psi}{\partial z}+\frac{1}{\rho}\frac{\partial p}{\partial z}+\frac{1}{8\pi\rho}\left(\frac{\partial B_{\phi}^{2}}{\partial z}+\frac{\partial B_{R}^{2}}{\partial z}\right)-\frac{1}{4\pi\rho}B_{R}\frac{\partial B_{z}}{\partial R}=0. \tag{28}$$

The self-gravitating case is also achievable through an elimination of the magnetic terms:

$$4\pi G\Sigma_{z}+\frac{\partial \Psi}{\partial z}+\frac{1}{\rho}\frac{\partial p}{\partial z}=0. \tag{29}$$

After regarding the similar considerations to get Equation (26), it can be written in the form of

$$2\pi G\rho_{0}^{2}H^{2}+\Omega^{2}\frac{\rho_{0}H^{2}}{2}+p_{0}(e^{-1/2}-1)=0. \tag{30}$$

2.2. Toomre Parameter

There are several numerical theoretical studies and simulations that describe a massive unstable disk in Newtonian gravity (e.g., Bonnell 1994; Matsumoto & Hanawa 2003) or even in modified gravity (e.g., Roshan & Abbassi 2015; Roshan et al. 2016). However, considering existing numerical simulations, it is not possible simply to say that all massive disks fragment because, to our knowledge, not only do current numerical simulations suffer from their own limitations, but they also do not generally give a fully consistent picture of global fragmentation. This situation gets more complicated when we consider magnetic fields. Apparently, the relation between gravitational instability and MHD turbulence is rather sophisticated; however, the more the MHD turbulence is getting highlighted, the less the gravitational instability is noticed (Fromang 2005; Shadmehri & Khajenabi 2006). Moreover, the fact that the accretion disks are differentially rotating opposes gravitational collapse. Anyway, it is the Toomre parameter that determines whether our NDAF is gravitationally unstable. In nonmagnetic literature, this criterion reads

$$Q=\frac{c_{s}\Omega_{k}}{\pi G\Sigma_{z}}, \tag{31}$$

where $Q<1$ implies instability. However, in the presence of magnetic field, this will be modified by a factor of $(1+\frac{\beta}{1-\beta})$ as follows (e.g., Shu 1992):

$$Q_{M}=Q\left(1+\frac{\beta}{1-\beta}\right), \tag{32}$$

where β has been introduced in Section 2.1.

2.3. "Magnetic Barrier" and/or "Fragmentation"?

Proposed by Proga & Zhang (2006), the mass accretion rate's decline during the late-time evolution of a hyperaccretion system can be considered as the source of unexpected X-ray flares in GRBs. They argued that the accumulated magnetic flux, in the inner edge of the disk, is capable of halting the accretion flow, intermittently. The importance of the magnetic effects for the X-ray flares can also be considered based on the energy budget of the accretion model (Fan et al. 2005). Following Xie et al. (2009), we take advantage of the comparison of the two timescales, namely, the diffusion and viscous timescales, in order to investigate the possibility of this process.

The magnetic field buoyancy and its rising time toward the disk surface can be estimated as

$$t_{\rm dif}\approx\frac{H}{v_{\rm A}}, \tag{33}$$

where $v_{\rm A}$ is the Alfvén velocity, $v_{\rm A}=\frac{B}{(4\pi\rho)^{1/2}}$. Besides, since the field lines are frozen to the disk materials, the viscous time t_{ν} can present the timescale of the magnetic flux accumulating in the vicinity of the black hole, and then we have

$$t_{\nu}=\int_{3R_{g}}^{R}\frac{1}{v_{R}}dR. \tag{34}$$

In the gravitational context, Perna et al. (2006) discussed that in the case of instabilities either a quasi-spiral structure may be imposed onto the disk by which the large-amplitude outbursts of accretion can be derived if the disk mass is sufficiently large (Laughlin et al. 1998; Lodato & Rice 2005), or the disk may fragment into bound objects. The latter is inevitable if (Gammie 2001; Perna et al. 2006)

$$t_{\rm cool}<t_{\rm cirt}\approx 3\Omega^{-1}, \tag{35}$$

where cooling timescale is denoted by $t_{\rm cool}\approx(H/R)^{2}t_{\nu}$ (Pringle 1981). Through such an analogy, the possibility of fragmentation can be verified in our model.

2.4. Neutrino Luminosity

After the neutrino cooling rate Q_{ν} is calculated, we are able to measure the neutrino luminosity, L_{ν}, which is expressed as

$$L_{\nu}=2\pi\int_{R_{\rm in}}^{R_{\rm out}}Q_{\nu}RdR, \tag{36}$$

where we adopt $R_{\rm in}=3R_{g}$ and $R_{\rm out}=200R_{g}$.

In the presence of strong magnetic field, it is also possible to extract the rotational energy of the disk or rotating black hole through ultrarelativistic GRB outflows driven by Pointing flux. BZ and BP processes are the two proposed mechanisms through which this purpose is fulfilled. The first suggests that the black hole rotational energy can be extracted by large-scale magnetic fields threading the horizon (Blandford & Znajek 1977). The latter asserts that an outflow of matter can be driven centrifugally by large-scale magnetic fields anchored at the surface of the disk (Blandford & Payne 1982). Hence, for the BP process the risk of baryonic pollution is much larger, as the wind originates from high-density regions (Daigne & Mochkovitch 2002). These winds of different Lorentz factors launched by BZ and BP processes compose a spine/sheath jet structure, which was first pointed out by Meier (2003) from observations and presented by Wang et al. (2008) to explain the jets for active galactic nuclei and black hole binaries. Nonetheless, following Xie et al. (2009), we consider the luminosity provided by this process since our central black hole is of the form of a Schwarzschild black hole, not a spinning one. The BP power output from a disk is equal to the power of disk magnetic braking and can be calculated as (Livio et al.

1999; Lee et al. 2000)

$$L_{\rm BP} = 2\pi \int_{R_{\rm in}}^{R_{\rm out}} Q_B R dR. \quad (37)$$

3. Numerical Results

As was pointed out in Section 2.1, our set of eight Equations (1), (2), (5), (15), (19), (20), (26), and (27) can be solved numerically, in which we have fixed $\alpha = 0.1$ and $M = 3\,M_\odot$. In spite of the inferred interval for constants β_1, β_2, γ_1, and γ_2, we estimate their values based on simulations such as those of Stone et al. (1996), from which one can deduce $\beta_1 \simeq \beta_2 \simeq 0.01$ and $\gamma_1 \simeq \gamma_2 \simeq 0.04$.

In Figure 1, for two different mass accretion rates ($\dot{M} = 0.1\,M_\odot\ {\rm s}^{-1}$ [left panels] and $\dot{M} = 10\,M_\odot\ {\rm s}^{-1}$ [right panels]), we have outlined the contours of density through the whole disk, with the gravitationally unstable regions ($Q < 1$) shaded in pink. We have considered self-gravitating magnetized NDAFs in the top two panels, the self-gravitating case in the middle two panels, and the magnetized case in the bottom two panels.

First of all, one can see that self-gravity has made the disk thinner, especially for the higher accretion rates and in the outer regions, where self-gravity plays an important role. It is also worth noting that the magnetic field has opposed the self-gravity and caused the disk scale height to increase. Second, the density drops by around three orders of magnitude when we go outward radially. In the case of self-gravitating magnetized NDAFs, the density is getting larger compared to the magnetized NDAFs. Of course, in agreement with Liu et al. (2014), such a behavior arises in the outer regions, and it is getting more obvious as the accretion rate grows. Furthermore, one can trace the gravitational instabilities ($Q < 1$) via the shaded realms in purple. Similar to Liu et al. (2014), as the mass accretion rate increases, the unstable realms grow inward, such that in the case of $\dot{M} = 0.1\,M_\odot\ {\rm s}^{-1}$ we do not encounter instability, but it is not the case for $\dot{M} = 10\,M_\odot\ {\rm s}^{-1}$. And last but not least, the magnetic field appears as a suppressor against gravitational instabilities, so that the unstable regions shrink when the magnetic effects come into play. This fully agrees with our expectations based on Section 2.2. To probe the possibility of fragmentation, we can make estimations for self-gravitating magnetized NDAFs based on the mentioned timescales in Section 2.3, i.e., cooling and critical timescales. In the outer disk, which is more likely to be gravitationally unstable, the cooling timescale is of the order of about 0.01 s for $\dot{M} = 4\,M_\odot\ {\rm s}^{-1}$ (that is the starting point at which instability occurs in the area of our interest) and about 0.001 s for $\dot{M} = 10\,M_\odot\ {\rm s}^{-1}$. These are obviously less than the critical timescale in the outer zones, which is of the order of 0.3 s. Thus, the fragmentation process would be a probable mechanism to make the mass accretion rate descend and, consequently, leads to the late-time X-ray flares, especially in the case of higher accretion rates.

The magnetic field components, B_R, B_ϕ, B_z, for the three mass accretion rates ($\dot{M} = 0.1,\ 1,\ 10\,M_\odot\ {\rm s}^{-1}$), have been plotted in Figure 2. Inwardly going through the disk, they show a rise of about two orders of magnitude, up to 10^{14}–10^{15} G, which is strong enough to power the most energetic GRBs with a luminosity of about $10^{53}\,{\rm erg\ s}^{-1}$. Furthermore, as self-gravity is taken into account, the magnetic field increases, which might reflect the dependency of the seed magnetic field's generation on the vertical density profile of the disk. This has been proposed by Safarzadeh et al. (2017), in which it is argued that the radial temperature profile and the vertical density profile of accretion disks provide the necessary conditions for the "Biermann battery" process (which is the mechanism responsible for the generation of the seed magnetic field) to operate naturally.

Figure 3 is an illustration of the velocity vector field on the disk's equatorial plane, for $\dot{M} = 10\,M_\odot\ {\rm s}^{-1}$, with some stream lines outlined. The change in colors expresses the variation of vectors' magnitude in logarithmic scale. Panel (a) includes the magnetic effects, as well as self-gravity. Comparing panel (a) with panel (b), in which self-gravity has been ignored, the velocity grows as an impact of self-gravity. On the other hand, panel (c) does not contain the magnetic field and instead considers the vertical self-gravity. Through an analogy between this panel and panel (a), one can find a reduction in velocity magnitude as the magnetic field comes into play.

The probability of "magnetic barrier" occurrence can be inferred from Figure 4, which provides us with the power of comparing the diffusion and viscous timescales for two mass accretion rates ($\dot{M} = 0.1,\ 10\,M_\odot\ {\rm s}^{-1}$), with and without self-gravity. First, in the lower accretion rates, the viscous time is sufficiently less than the diffusion time, which can enhance the chance of magnetic field accumulation and subsequently the magnetic barrier. Next, in the absence of vertical self-gravity, the diffusion time experiences an increase in the outer regions, where the self-gravity appears to be more effective. Such an effect implies that the vertical diffusion or buoyancy process is facilitated by self-gravity since it makes the disk thinner. Yet, it seems to have no effect on the viscous timescale, which reveals the fact that we have just considered the $r\phi$-component of the viscous stress tensor. Moreover, as the mass accretion rate increases, which leads to a growth in density and a drop in the disk scale height (Figure 1), both diffusion and viscous timescales decline. Lastly, in the case of higher accretion rates, self-gravity may suppress the magnetic barrier.

The zones dominated by each of the cooling rates (i.e., neutrino, advection and magnetic field fractions), in the R–$\dot{M}$ plane, are presented in Figure 5. Panel (a) considers both self-gravity and magnetic field, and panel (b) is related to the magnetic effects. Also, it should be mentioned that the green and black boundaries, with their contours of the $Q_B/Q_{\rm vis}$ ratio, correspond to the magnetic-cooling-dominated realms over advective and neutrino processes, respectively. The contours in purple display neutrino-dominated regions over all other cooling processes. And orange contours correspond to the advection-dominated areas over two other cooling mechanisms. Generally speaking, neutrino cooling gets highlighted over an extended area. Moreover, the advective cooling rate becomes more effective as self-gravity is taken into account, especially in the outer disk, which is more affected by self-gravity. Such an outcome might arise as a result of a growth in density, and subsequently the generated magnetic field will grow. This causes the magnetic process to become more efficient in the outer disk, as well. Figure 6 is an illustration of BP power and neutrino luminosity versus mass accretion rate throughout the disk. Both cases seem to be strong enough to power the GRB jets. On the other hand, the smooth downward trend of neutrino cooling efficiency (Figure 7; $\eta_\nu = L_\nu/\dot{M}c^2$, with which energy is transported out of the flow by neutrinos) can display the reduction of neutrinos' capability to cool the disk. Such a

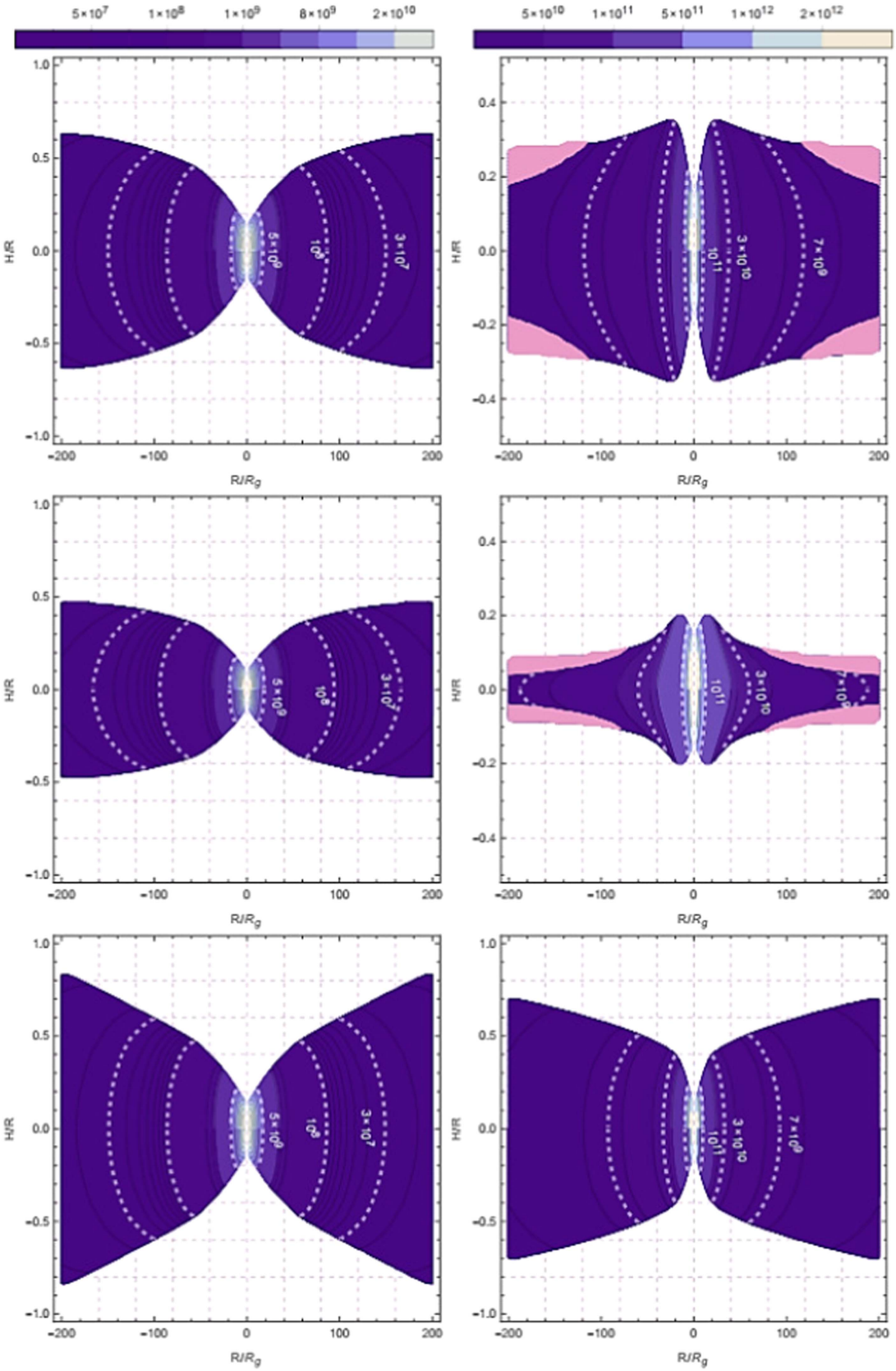

Figure 1. Contours of density for $\dot{M} = 0.1\,M_{\odot}\,\mathrm{s}^{-1}$ (left) and $\dot{M} = 10\,M_{\odot}\,\mathrm{s}^{-1}$ (right), with three orders of density highlighted by dashed lines (5×10^9, 10^8, 3×10^7 g cm^{-3} for the left panels; 10^{11}, 3×10^{10}, 7×10^9 g cm^{-3} for the right panels). The top two panels are devoted to the self-gravitating magnetized NDAF, the middle two panels are related to the self-gravitating case, and the bottom two panels show the magnetized NDAF. Additionally, the shaded areas in pink show the gravitationally unstable zones.

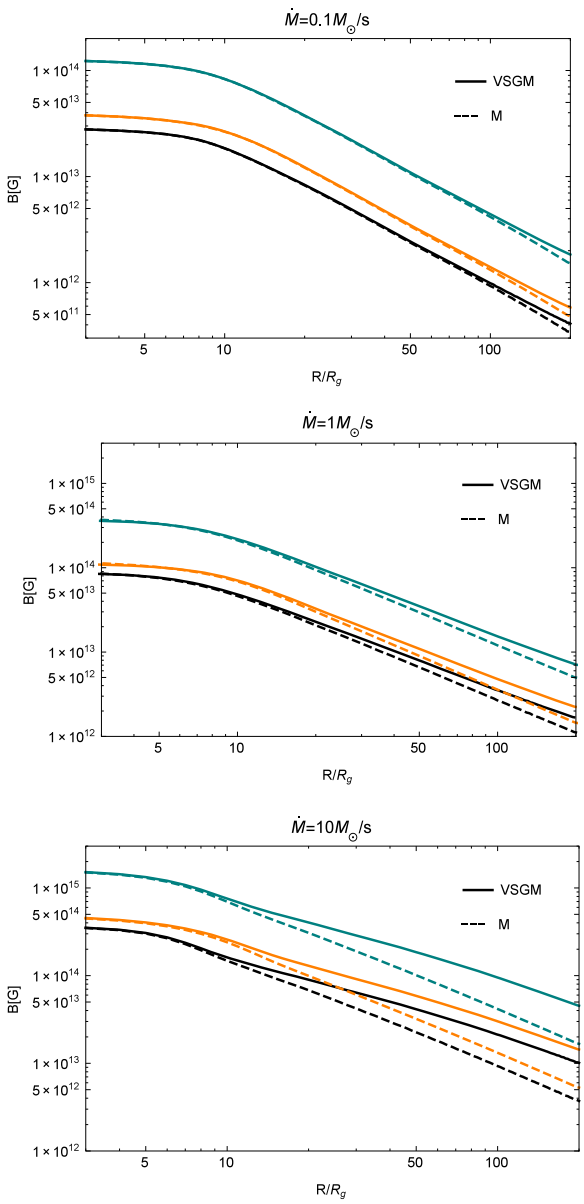

Figure 2. Magnetic field components, B_R, B_ϕ, B_z, for two cases of magnetized NDAFs: with (VSGM) and without self-gravity (M) (solid and dashed curves, respectively). In these three panels, the radial, azimuthal, and poloidal components are plotted in orange, blue, and black, respectively.

decline is caused by the increase of neutrino opacity for higher accretion rates (Di Matteo et al. 2002). This leads neutrinos to be more trapped. Furthermore, self-gravity appears to play opposite roles in two cases (BP power and neutrino luminosity). That is to say, it has lessened the luminosity of neutrinos, which is in contrast to the Liu et al. (2014) outcomes, but has enhanced the BP power. This unexpected behavior reflects the fact that self-gravity increases BP power more than neutrino luminosity. For one thing, neutrino emission occurs more in the inner disk, but it is the outer regions that are more affected by self-gravity. For another, self-gravity increases the generated magnetic field and, consequently, highlights its role in cooling the disk, which may weaken the fraction of neutrinos.

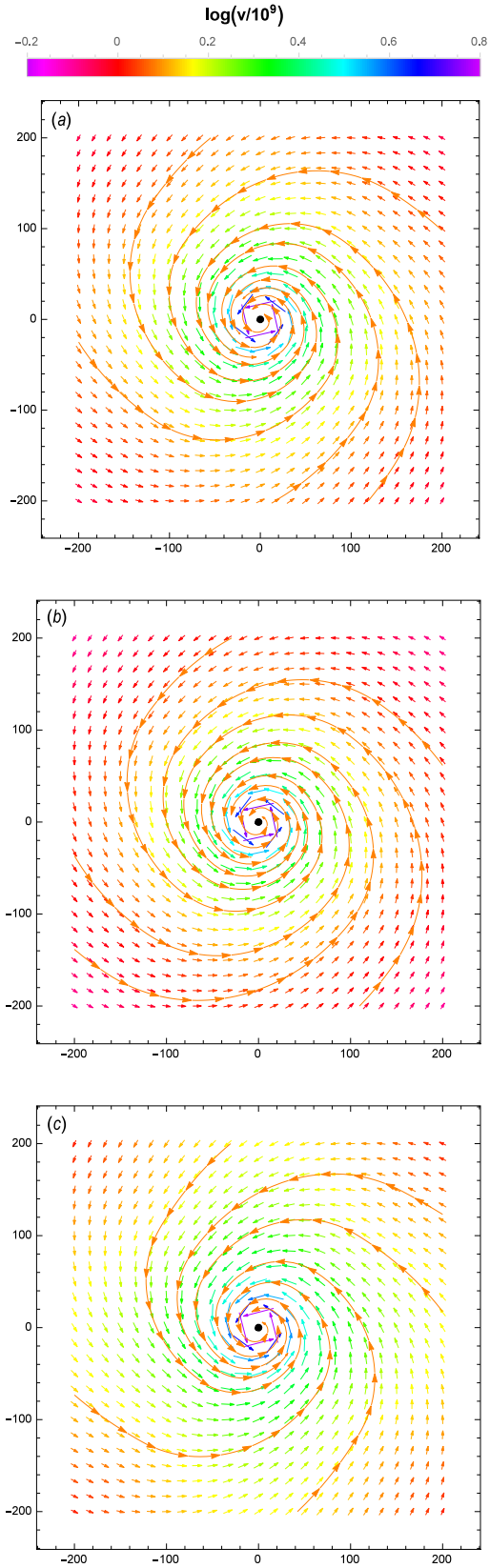

Figure 3. Illustration of velocity vector field (cm s^{-1}) on the disk's equatorial plane, for $\dot{M} = 10\,M_\odot$ s^{-1}, with some stream lines outlined. In panel (a) both self-gravity and magnetic field have been included, but it is the magnetic field that governs the disk in panel (b). Panel (c) only covers the self-gravity impacts.

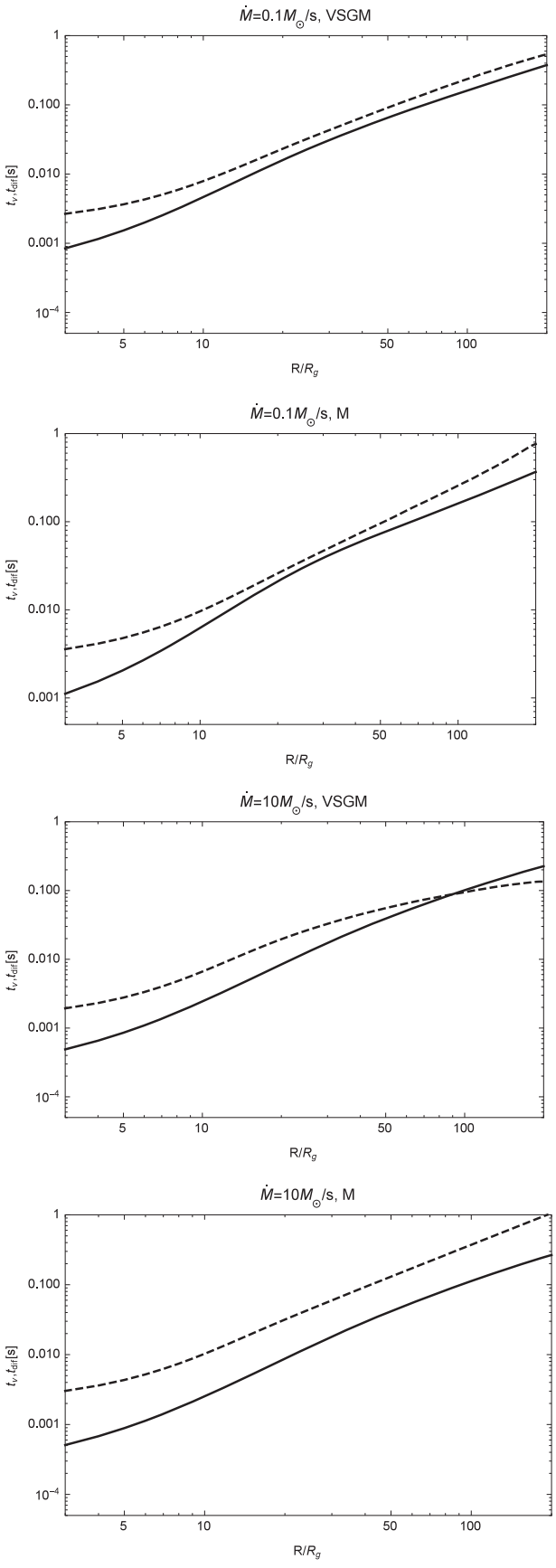

Figure 4. Viscous and diffusion timescales for $\dot{M} = 0.1,\ 10\ M_\odot\ \mathrm{s}^{-1}$ illustrated by solid and dashed lines. Both magnetized (M) and vertically self-gravitating magnetized (VSGM) cases are considered.

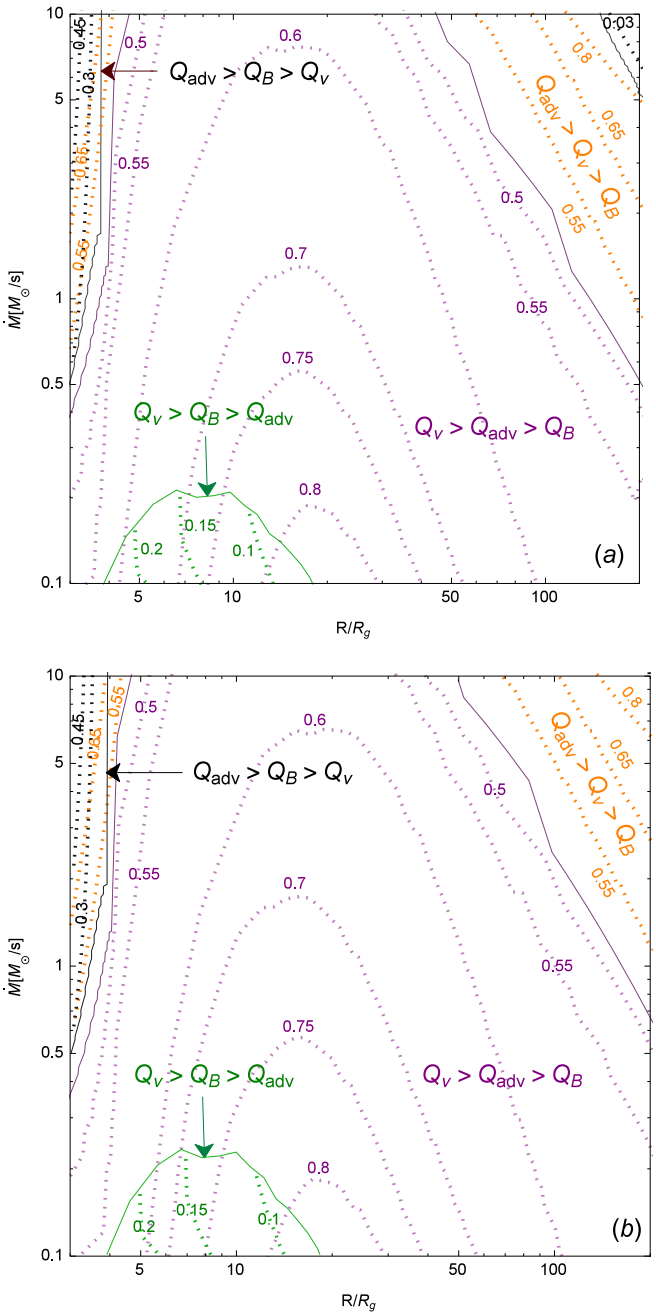

Figure 5. Contours of three different cooling rates' ratios with respect to viscous cooling rate (i.e., $Q_{\rm adv}/Q_{\rm vis}$, $Q_B/Q_{\rm vis}$, and $Q_\nu/Q_{\rm vis}$), in the R–$\dot{M}$ plane. The boundaries of their dominance are shown with solid lines. Panel (a) is the case for self-gravitating magnetized NDAFs, whereas panel (b) represents the magnetized one.

Ignoring the nucleons' degeneracy, there might be some points worth noting. First, Kohri & Mineshige (2002) have argued that the nucleon degeneracy, in contrast to that of electrons, has a suppressing effect on the neutrino cooling rate, and this subsequently lowers the neutrino luminosity and its efficiency. The second is how fragmentation and the magnetic barrier would be affected by such a consideration. We think that, since the nature of degeneracy pressure is opposed to the density enhancement due to self-gravity, the possibility of fragmentation should drop if the nucleon degeneracy is taken into account. This might be the same for the magnetic barrier,

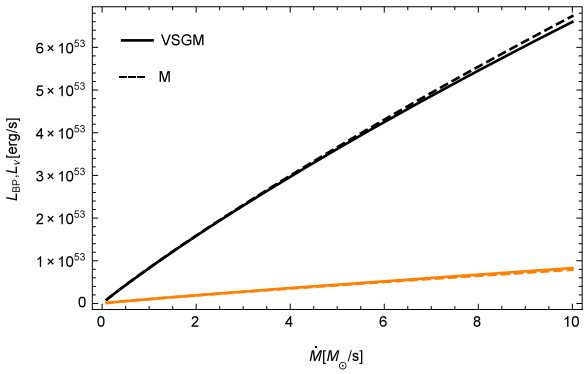

Figure 6. Neutrino luminosity and BP power (black and orange lines) vs. mass accretion rate. Solid lines represent the magnetized NDAF with vertical self-gravity (VSGM), but in dashed lines it is ignored (M).

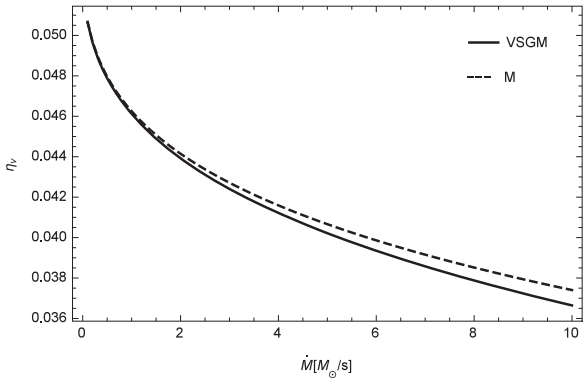

Figure 7. Neutrino cooling efficiency vs. mass accretion rate. Solid and dashed curves display the magnetized NDAF considering (VSGM) and ignoring self-gravity (M), respectively.

in which the nucleon degeneracy will result in an increase in the disk's pressure, and consequently the density will grow (consider the polytropic EOS). Of course, this relation might be inferable from Kohri & Mineshige (2002), which confirms that the denser regions correspond to the realms with higher nucleon degeneracy importance. This can lead to a stronger magnetic field, as Figure 2 reflects such an impact. Thus, the magnetic barrier might become less probable owing to a decrease in diffusion timescale and a growth in viscous timescale, each of which is a result of the stronger magnetic field.

4. Estimates and Observational Evidence

In this section, following Proga & Zhang (2006), we provide estimates of some of the features of X-ray flares. As a first step, regarding our results, we calculate the magnetic flux accumulated in the vicinity of the black hole and test whether it has the capability to result in the X-ray flares. Taking the magnetic barrier into account, the radial magnetic force, $F_m \approx 2B_R B_z/4\pi$, should balance the gravitational one, $F_g = GM_b\Sigma/R^2$, to support the infalling gas. $\Sigma = \dot{M}/(2\pi R\epsilon v_{ff})$ is the surface density of the gas, and ϵv_{ff} is the flow radial velocity, assumed to be a fraction ϵ of the freefall velocity, $v_{ff} = (2GM_b/R)^{1/2}$ (we refer readers to Narayan et al. (2003) for more information about "magnetically arrested disk"). Assuming $B_R \approx B_z = B$, which is approximately consistent with the simulation results we have applied, the force balance yields the magnetic flux as $\Phi \approx \pi R^2 B(r) = 5 \times 10^{28}\epsilon_{-3}^{-1/2}(R/R_g)^{3/4}\dot{M}_1^{1/2}M_3$ cm^2 G, where $\epsilon_{-3} = 10^3\epsilon$, $\dot{M}_1 = \dot{M}/1\ M_\odot\ \mathrm{s}^{-1}$, and $M_3 = M_b/3\ M_\odot$. The magnetospheric radius, at which the accumulated poloidal field disrupts the accretion flow, and lying well outside the event horizon of the black hole, can be estimated as $r_m \approx 60\epsilon_{-3}^{2/3}\dot{M}_1^{-2/3}M_3^{-4/3}\Phi_{30}^{4/3}$, where $\Phi_{30} \equiv \Phi/(10^{30}\ \mathrm{cm}^2\ \mathrm{G})$.

To estimate the conditions needed to restart accretion, the accretion energetics, and related timescales, we ask what is the mass of a disk with Σ high enough to reduce r_m from its own magnitude in the late-time evolution to 3 or so. Before that, we should make an estimation for r_m in the late-time disk's activity. Although there are different strategies in the literature for making this estimate (e.g., Lloyd-Ronning et al. 2016; Tchekhovskoy et al. 2014), we continue to follow Proga & Zhang (2006). In the case that the hyper-rate of $10\ M_\odot\ \mathrm{s}^{-1}$ onto the black hole is considered, regarding the flux definition, the accumulated magnetic flux at $r = R/R_g = 3$ would be of the order of $\Phi_{30} \approx 0.02$. Now, we assume that such a magnetic flux is accumulated during hyperaccretion and that it does not change with time. On the other hand, Yi et al. (2016) have found that the 0.3–10 keV isotropic energy of X-ray flares is mainly distributed from 10^{50} to 10^{52} erg, which is more than two orders of magnitude less than that of the prompt emission of GRBs. Therefore, leading to $r_m = 33$, the adoption of $10^{-3}\ M_\odot\ \mathrm{s}^{-1}$ for the late-time evolution mass supply rate seems to be a reasonable choice. Another assumption that we made is the value of 10^{-3} for ϵ. Indeed, this parameter is on less firm footing (for more discussion of this parameter and its physical importance, see, e.g., McKinney et al. 2003; Narayan et al. 2003; Lloyd-Ronning et al. 2016).

Now we can make our estimates for the duration timescales of the late-time activities. With $\Phi_{30} \approx 0.02$, the accretion rate would be about $0.04\ M_\odot\ \mathrm{s}^{-1}$. Clearly, this accretion rate is around three orders of magnitude less than the rate $\dot{M} = 10\ M_\odot\ \mathrm{s}^{-1}$. Thus, our outcome is well consistent with observations studied by Yi et al. (2016). On the other hand, the disk mass for r between 3 and 33 would be about $0.25\ M_\odot$. If this disk mass is a result of slow mass accumulation during the late evolutionary stage, then it will take about 250 s to rebuild the disk for the mass supply rate of $10^{-3}\ M_\odot\ \mathrm{s}^{-1}$ and 6 s to accrete all this mass at the disk accretion rate of $0.04\ M_\odot\ \mathrm{s}^{-1}$. The former lies between 100 and 1000 s, the interval that has been inferred as the duration time of the flares by Yi et al. (2016). However, the latter might be an underestimated value of the flare duration, since we assumed a relatively high constant accretion rate, which is obviously opposed to the time dependency of the light curves' behavior during the flare.

Although our model seems to be capable of predicting outcomes compatible with the observed duration timescale, there are some considerations to keep in mind. Besides being affected by some other factors like rotation (Lloyd-Ronning et al. 2016), we are of the opinion that the magnetospheric radius should be influenced by the fragmentation. This process will lower the disk accretion rate, which might result in a larger magnetospheric radius (inferable from the r_m relation) and, subsequently, in a longer duration timescale. Of course, such a correlation appears to agree with the observational evidences found by Ramirez-Ruiz & Merloni (2001) and the analytical estimates studied by Lloyd-Ronning et al. (2016), in which the quiescent time–pulse duration correlation has been discussed. Finally, in agreement with our previous results (deduced from Figure 4), the fragmentation process might lower the magnetic barrier effectiveness to produce X-ray flares.

5. Conclusions

We study the structure and evolution of neutrino-dominated accretion disks, in which the consideration of self-gravity and magnetic field provides us with a more realistic picture of these central engines of GRBs. We find self-gravity to be a booster of magnetic field, mainly in the outer disk. Such an effect, especially in higher accretion rates, enhances the BP power and decreases the neutrino luminosity fraction. The latter is contrary to Liu et al. (2014) outcomes but seems a natural result of the strong magnetic field presence as we discussed formerly. On the other hand, the probable fragmentation process lessens the magnetic barrier possibility by a decrease in magnetic field diffusion timescale for higher mass accretion rates. This result can also be deduced from the estimations we have already made and their comparison with the observational evidences.

On the whole, we find both MHD and neutrino processes effective enough (10^{50-54} erg s^{-1}) to produce GRBs' spectrum. Of course, in the case of higher accretion rates, the drop in neutrino efficiency (Figure 7), as a result of a growth in neutrino opacity, may confirm a decrease in neutrinos' capability to transport the energy outside. In the context of late-time X-ray flares, the magnetic barrier process would be more probable to power such extended emissions in low accretion rates, because fragmentation is less likely to happen. Yet, this might not be the case for higher accretion rates, as fragmentation can overcome the magnetic barrier to produce energetic X-ray flares.

Nevertheless, what is presented in this work might be a simplified model from the central engines of GRBs that should be improved by the consideration of all other physical aspects of these engines. For instance, the unsteady structure of NDAFs, resulting in jets with shells of different Lorentz factor, can realize our physical perception of NDAFs (as proposed by Narayan et al. 1992; Meszaros & Rees 1994; Paczynski & Xu 1994). The fact that viscous timescales in the inner disk, where all the neutrino processes become important, are shorter than those in the outer disk, where $\dot{M}$ is expected to vary (inferable from Figure 4), justifies applying the steady approximation (Di Matteo et al. 2002); however, the time-dependent behavior of the GRB engine, as well as the probable instabilities, makes the unsteady state a more viable approach. Or, considering the fully self-gravitating magnetized NDAF might enhance the validity of our estimations and results. On the other hand, several other mechanisms make efforts to describe X-ray flares, such as fragmentation of a rapidly rotating core (King et al. 2005), differential rotation in a post-merger millisecond pulsar (Dai et al. 2006), He-synthesis-driven wind (Lee et al. 2009), jet precession (Liu et al. 2010b), and episodic jets produced by the magnetohydrodynamic mechanism from the accretion disk (Yuan & Zhang 2012), all of which might lead us to different outcomes.

One more point that deserves mentioning is that the high rotation, required to form the centrifugally supported disk that powers the GRB, should produce gravitational waves via bar (e.g., Dimmelmeier et al. 2008) or fragmentation instabilities that might develop in the collapsing core (see, e.g., Ott 2009) and/or in the disk (Kobayashi & Meszaros 2003; Piro & Pfahl 2007). This gives our model the potential to affect the predictions and estimations made in the context of gravitational waves, which might be another complementary discussion worth noting for future studies.

Anyway, considering such a variety of models or physical features, more information from the multiband observations and the detections on the polarization and gravitational waves on the GRBs and their flares is needed to decide which model or what physical conditions can provide us with a more accurate insight into the enigmatic nature of GRBs.

We are grateful to the constructive and thoughtful comments of the referee, which helped us to improve an earlier version of this article. This work was supported by the Ferdowsi University of Mashhad under grant no. 43650 (1396/02/6).

ORCID iDs

Shahram Abbassi https://orcid.org/0000-0003-0428-2140

References

Balbus, S. A., & Hawley, J. F. 1991, ApJ, 376, 214
Blandford, R. D. 1976, MNRAS, 176, 465
Blandford, R. D., & Payne, D. G. 1982, MNRAS, 199, 883
Blandford, R. D., & Znajek, R. L. 1977, MNRAS, 179, 433
Bonnell, I. A. 1994, MNRAS, 269, 837
Cao, X., Liang, E. W., & Yuan, Y. F. 2014, ApJ, 789, 129
Dai, Z. G., Wang, X. Y., Wu, X. F., & Zhang, B. 2006, Sci, 311, 1127
Daigne, F., & Mochkovitch, R. 2002, A&A, 388, 189
Di Matteo, T., Perna, R., & Narayan, R. 2002, ApJ, 579, 706
Dimmelmeier, H., Ott, C. D., Marek, A., & Janka, H.-T. 2008, PhRvD, 78, 064056
Eichler, D., & Cheng, A. F. 1989, ApJ, 336, 360
Fan, Y. Z., Zhang, B., & Proga, D. 2005, ApJ, 635L, 129
Fromang, S. 2005, A&A, 441, 1
Fryer, Chris L., & Woosley, S. E. 1998, ApJ, 501, 780
Gammie, C. F. 2001, ApJ, 553, 174
Gehrels, N., Ramirez-Ruiz, E., & Fox, D. B. 2009, ARA&A, 47, 567
Gu, W. M., Liu, T., & Lu, J. F. 2006, ApJ, 643L, 87
Gu, W. M., Liu, T., & Lu, J. F. 2007, ASPC, 373, 135
Gu, W. M., Xue, L., Liu, T., & Lu, J. F. 2009, PASJ, 61, 1313
Hjorth, J., Sollerman, J., Moller, P., et al. 2003, Natur, 423, 847
Jiao, C. L., Xue, L., Gu, W. M., & Lu, J. F. 2009, ApJ, 693, 670
Kato, S., Fukue, J., & Mineshige, S. 2008, Black-Hole Accretion Disks: Towards a New Paradigm (Kyoto: Kyoto Univ. Press)
King, A., O'Brien, P. T., Goad, M. R., et al. 2005, ApJL, 630, L113
Kobayashi, S., & Meszaros, P. 2003, ApJ, 589, 861
Kohri, K., & Mineshige, S. 2002, ApJ, 577, 311
Kohri, K., Narayan, R., & Piran, T. 2005, ApJ, 629, 341
Kouveliotou, C., Meegan, C. A., Fishman, G. J., et al. 1993, ApJ, 413L, 101
Kumar, P., & Zhang, B. 2015, PhR, 561, 1
Laughlin, G., Korchagin, V., & Adams, F. C. 1998, ApJ, 504, 945
Lee, H. K., Wijers, R. A. M. J., & Brown, G. E. 2000, Phys. Rev, 325, 83
Lee, W. H., Ramirez-Ruiz, E., & Lopez-Camara, D. 2009, ApJL, 699, L93
Lei, W. H., Wang, D. X., Zhang, L., et al. 2009, ApJ, 700, 1970
Liu, T., Gu, W. M., Dai, Z. G., & Lu, J. F. 2010a, ApJ, 709, 851
Liu, T., Gu, W. M., Xue, L., & Lu, J. F. 2007, ApJ, 661, 1025
Liu, T., Gu, W. M., & Zhang, B. 2017, arXiv:1705.05516
Liu, T., Liang, E. W., Gu, W. M., et al. 2010b, A&A, 516, A16
Liu, T., Yu, X. F., Gu, W. M., & Lu, J. F. 2014, ApJ, 791, 69
Livio, M., Ogilvie, G. I., & Pringle, J. E. 1999, ApJ, 512, 100
Lloyd-Ronning, N. M., Dolence, J. C., & Fryer, C. L. 2016, MNRAS, 461, 1045
Lodato, G., & Rice, W. K. M. 2005, MNRAS, 358, 1489
Matsumoto, T., & Hanawa, T. 2003, ApJ, 595, 913
McKinney, J. C., Tchekhovskoy, A., & Blandford, R. D. 2003, MNRAS, 423, 3083
Meier, D. L. 2003, NewAR, 47, 667
Meszaros, P. 2006, RPPh, 69, 2259
Meszaros, P., & Rees, M. J. 1994, AIPC, 307, 505
Meszaros, P., & Rees, M. J. 1997, ApJ, 476, 232
Nakar, E. 2007, PhR, 442, 166
Narayan, R., Igumenshchev, I. V., & Abramowicz, M. A. 2003, PASJ, 55L, 69
Narayan, R., Paczynski, B., & Piran, T. 1992, ApJ, 395L, 83
Narayan, R., Piran, T., & Kumar, P. 2001, ApJ, 557, 949
Ott, C. D. 2009, CQGra, 26, 063001
Paczynski, B. 1978a, AcA, 28, 91

Paczynski, B. 1978b, AcA, 28, 241
Paczynski, B. 1998, AIPC, 428, 783
Paczynski, B., & Xu, G. 1994, ApJ, 427, 708
Paczynsky, B., & Wiita, P. J. 1980, A&A, 88, 23
Perna, R., Armitage, P. J., & Zhang, B. 2006, ApJ, 636L, 29
Piran, T. 2004, RvMP, 76, 1143
Piro, A. L., & Pfahl, E. 2007, ApJ, 658, 1173
Popham, R., Woosley, S. E., & Fryer, C. 1999, ApJ, 518, 356
Pringle, J. E. 1981, ARA&A, 19, 137
Proga, D., & Zhang, B. 2006, MNRAS, 370L, 61
Qian, Y. Z., & Woosley, S. E. 1996, ApJ, 471, 331
Ramirez-Ruiz, E., & Merloni, A. 2001, MNRAS, 320, L25
Roshan, M., & Abbassi, S. 2015, Ap&SS, 358, 11
Roshan, M., Abbassi, S., & Khosroshahi, H. G. 2016, ApJ, 832, 201
Safarzadeh, M., Naoz, S., Sadowski, A., Sironi, L., & Narayan, R. 2017, arXiv:1701.03800
Shadmehri, M., & Khajenabi, F. 2006, ApJ, 637, 439
Shakura, N. I., & Sunyaev, R. A. 1973, A&A, 24, 337
Shibata, M., Sekiguchi, Y. I., & Takahashi, R. 2007, PThPh, 118, 257
Shu, F. H. 1992, The Physics of Astrophysics, Vol. 2 (Mill Valley: Univ. Science Books)
Stone, J. M., Hawley, J. F., Gammie, C. F., & Balbus, S. A. 1996, ApJ, 463, 656
Tchekhovskoy, A., Metzger, B. D., Giannios, D., & Kelley, L. Z. 2014, MNRAS, 437, 2744
Usov, V. V. 1992, Natur, 357, 472
Wang, D. X., Ye, Y. C., Li, Y., & Ge, Z. J. 2008, MNRAS, 385, 841
Woosley, S. E. 1993, ApJ, 405, 273
Woosley, S. E., & Baron, E. 1992, ApJ, 391, 228
Xie, Y., Huang, Z. Y., Jia, X. F., Fan, S. J., & Liu, F. F. 2009, MNRAS, 398, 583
Yi, S. X., Xi, S. Q., Yu, H., et al. 2016, ApJS, 224, 20
Yu, Y. W., Zhang, B., & Gao, H. 2013, ApJ, 776L, 40
Yuan, F., & Zhang, B. 2012, ApJ, 757, 56